



**HAL**  
open science

# A plastic aggrecan barrier modulated by peripheral energy state gates metabolic signal access to arcuate neurons

Laura Kuczynski-Noyau, Sixtine Karmann, Paolo Alberton, Ines Martinez-Corral, Sreekala Nampoothiri, Florent Sauv , Tori Lhomme, Carmelo Quarta, Suneel Apte, S bastien Bouret, et al.

## ► To cite this version:

Laura Kuczynski-Noyau, Sixtine Karmann, Paolo Alberton, Ines Martinez-Corral, Sreekala Nampoothiri, et al.. A plastic aggrecan barrier modulated by peripheral energy state gates metabolic signal access to arcuate neurons. *Nature Communications*, 2024, 15 (1), pp.6701. 10.1038/s41467-024-50798-9. hal-04747436

**HAL Id: hal-04747436**

**<https://hal.science/hal-04747436v1>**

Submitted on 25 Oct 2024

**HAL** is a multi-disciplinary open access archive for the deposit and dissemination of scientific research documents, whether they are published or not. The documents may come from teaching and research institutions in France or abroad, or from public or private research centers.

L'archive ouverte pluridisciplinaire **HAL**, est destin e au d p t et   la diffusion de documents scientifiques de niveau recherche, publi s ou non,  manant des  tablissements d'enseignement et de recherche fran ais ou  trangers, des laboratoires publics ou priv s.



Distributed under a Creative Commons Attribution - NonCommercial - NoDerivatives 4.0 International License

# A plastic aggrecan barrier modulated by peripheral energy state gates metabolic signal access to arcuate neurons

Received: 12 March 2024

Accepted: 17 July 2024

Published online: 07 August 2024


 Check for updates

Laura Kuczynski-Noyau <sup>1,7</sup>, Sixtine Karmann <sup>1,7</sup>, Paolo Alberton <sup>2,3</sup>, Ines Martinez-Corral <sup>1</sup>, Sreekala Nampoothiri <sup>1</sup>, Florent Sauv   <sup>1</sup>, Tori Lhomme <sup>1</sup>, Carmelo Quarta <sup>4</sup>, Suneel S. Apte <sup>5</sup>, S  bastien Bouret <sup>1</sup>, Attila Aszodi <sup>2</sup>, Sowmyalakshmi Rasika <sup>1</sup>, Philippe Ciofi <sup>4</sup>, Julie Dam <sup>6</sup>, Vincent Pr  vot <sup>1</sup> & Virginie Mattot <sup>1</sup> 

The hypothalamic arcuate nucleus (ARH) contains neurons vital for maintaining energy homeostasis that sense and respond to changes in blood-borne metabolic hormones. Despite its juxtaposition to the median eminence (ME), a circumventricular organ lacking a blood-brain barrier and thus exposed to circulating molecules, only a few ventral ARH neurons perceive these extravasating metabolic signals due to a poorly understood ME/ARH diffusion barrier. Here, we show in male mice that aggrecan, a perineural-net proteoglycan deposited by orexigenic ARH neurons, creates a peculiar ventrodorsal diffusion gradient. Fasting enhances aggrecan deposition more dorsally, reinforcing the diffusion barrier, particularly around neurons adjacent to fenestrated capillary loops that enter the ARH. The disruption of aggrecan deposits results in unregulated diffusion of blood-borne molecules into the ARH and impairs food intake. Our findings reveal the molecular nature and plasticity of the ME/ARH diffusion barrier, and indicate its physiological role in hypothalamic metabolic hormone sensing.

The cross-talk between the periphery and the brain is essential to maintain energy homeostasis. At the core of this cross-talk, neurons located in the arcuate nucleus of the hypothalamus (ARH), including the orexigenic neuropeptide Y (NPY)- and agouti-related peptide (AgRP)-expressing neurons and the anorexigenic proopiomelanocortin (POMC)-expressing neurons<sup>1,2</sup>, must integrate numerous blood-borne metabolic signals from the periphery to induce a suitable tissue-specific response to changing conditions. The ARH is located just above the median eminence (ME)<sup>1,2</sup>, a circumventricular organ vascularized by a dense network of fenestrated capillaries that, unlike typical capillaries of the blood-brain barrier, allow the free diffusion of molecules into the

brain parenchyma<sup>3</sup>. A subset of NPY/AgRP neurons is present in the ventromedial ARH precisely at the border with the ME<sup>1,2</sup>, a position that exposes them to peripheral blood-borne molecules extravasating from ME microvessels and diffusing into the parenchyma<sup>4</sup>. However, a long-described diffusion barrier prevents the free and homogeneous passage of blood-borne molecules, including metabolic signals important for the central regulation of energy homeostasis, between the ME and the rest of the ARH<sup>5-12</sup>. The precise nature of this barrier remains incompletely understood and its potential regulation is unexplored, posing a significant obstacle to our understanding of this regulation and its disruption in metabolic diseases.

<sup>1</sup>Univ. Lille, INSERM, CHU Lille, Laboratory of Development and Plasticity of the Neuroendocrine Brain, Lille Neuroscience & Cognition, UMR-S1172, EGID, Lille, France. <sup>2</sup>Department for Orthopaedics and Trauma Surgery Musculoskeletal University Center Munich (MUM) University Hospital, LMU, Munich, Germany. <sup>3</sup>Division of Hand, Plastic and Aesthetic Surgery LMU University Hospital, LMU, Munich, Germany. <sup>4</sup>Univ. Bordeaux, INSERM, Neurocentre Magendie, U1215, Bordeaux, France. <sup>5</sup>Department of Biomedical Engineering, Cleveland, OH, USA. <sup>6</sup>Institut Cochin, INSERM, CNRS, Universit   Paris Cit  , Paris, France. <sup>7</sup>These authors contributed equally: Laura Kuczynski-Noyau, Sixtine Karmann.  e-mail: [virginie.mattot@inserm.fr](mailto:virginie.mattot@inserm.fr)

At the ME/ARH border, NPY/AgRP neurons are embedded in a specialized extracellular matrix resembling the perineural net (PNN)<sup>13–17</sup>. The PNN is a condensed matrix composed of a scaffold of glycosaminoglycans (hyaluronan) to which proteoglycans (especially chondroitin sulfate proteoglycans such as aggrecan, versican, neurocan and brevican) attach, and are stabilized by proteins (hyaluronan and proteoglycan binding link proteins – Haplns – or Tenascin)<sup>18</sup>. The PNN enwraps neuronal somata and proximal axonal and dendritic extensions<sup>18</sup>, generating an ion gradient<sup>19</sup>, interfering with cell signaling<sup>18</sup> or maintaining a non-plastic state for PNN-enmeshed neurons<sup>20</sup>. At the ME/ARH border, the deposition of the PNN is developmentally regulated, being sensitive to the postnatal surge of the adipose tissue-derived metabolic hormone leptin<sup>13</sup>, also known to sculpt ARH projections<sup>21</sup> and the stability of the PNN network in adulthood appears to be regulated by gonadal hormones in both male and female mice<sup>22</sup>. Evidence indicates that the PNN undergoes alteration at the ME/ARH border in metabolic diseases such as obesity and type 2 diabetes<sup>13,14,22</sup>, while the presence of an intact PNN at this site is essential for achieving diabetes remission<sup>14</sup>.

Proceeding from the aforementioned observations, we asked whether the PNN could constitute the diffusion barrier between the ME and the ARH, and investigated its role in modulating the access of ARH neurons regulating energy homeostasis to blood-borne metabolic signals. In the present study, we show that aggrecan is a PNN component deposited precisely at the location of the diffusion barrier at the ME/ARH boundary, where it controls the diffusion of blood-borne molecules, creating a gradient. In fasting mice, aggrecan deposits extend dorsally to surround a subpopulation of NPY neurons juxtaposed to fenestrated blood vessels originating from the ME and through which circulating signals extravasate into the ARH, further controlling their access to their target neurons. The genetic or enzymatic disruption of aggrecan deposition leads to the uncontrolled diffusion of blood-borne molecules into the ARH and the dysregulation of food intake both after an acute ghrelin injection and during physiological refeeding. The molecular nature of the long-described ME/ARH diffusion barrier and its energy state-dependent plasticity indicate a role for the PNN in the hypothalamic sensing of metabolic signals and the regulation of energy homeostasis.

## Results and discussion

To explore the mechanisms underlying the specific distribution of blood-borne molecules at the ME/ARH frontier, we first studied the spatial spread of fluorescent dextrans in the ARH 5 min after their injection into the bloodstream. In mouse brain sections, we found that the diffusion of 10 kDa dextran, and even that of 3 kDa, representing the molecular weight of ghrelin, a peripheral metabolic hormone that extravasates into the ME, is abruptly restrained after their entry in the ME (Fig. 1a). This sharp impediment to dextran diffusion towards the ARH was validated by plotting the intensity of dextran fluorescence along a ventrodorsal ME-ARH axis (Fig. 1a). To verify whether this distinct spatial diffusion pattern of circulating molecules also applies to endogenous blood-borne signals, we examined the distribution of ~65-kDa albumin. This protein, abundant in the plasma, acts as a carrier for circulating peptides, notably ghrelin, shielding them from inactivation<sup>23,24</sup>. Furthermore, previous studies have demonstrated albumin extravasation from fenestrated capillaries in the ME and its diffusion into the ARH<sup>4,25</sup>. Using immunofluorescence labeling of endogenous albumin on *NPY-GFP* mouse brain sections and plotting its intensity along an ME-ARH axis (Fig. 1b), we observed that albumin levels also suddenly dropped at the ME/ARH border. This drop was associated with the presence of orexigenic GFP-labeled NPY neurons (Fig. 1b) but did not match with that of vimentin-positive cellular processes (running along the ME/ARH border and originating from specialized ependymogial tanycytes forming the ventral and lateral walls of the third ventricle) or that of POMC anorexigenic neurons

(Supplementary Fig. 1a, b). Interestingly, as more frequently observed in the most caudal extension of the ME/ARH, albumin was also detected in a contained dorsal area of the ARH bordering the wall of the third ventricle, where a subset of NPY neurons is contacted by ME capillary loops that penetrate the ARH and are known to become fenestrated in response to fasting<sup>26</sup> (Fig. 1c). Since the distribution pattern of endogenous albumin mirrored that of blood-borne low molecular weight dextrans, we proceeded to use albumin as a proxy for peripheral metabolic signals. This allowed us to assess the integrity of the diffusion barrier at the ME/ARH frontier.

As the diffusion of molecules in the brain occurs predominantly through the extracellular space<sup>27</sup>, we next investigated whether the density of the PNN, a specialized extracellular matrix in which NPY neurons are embedded<sup>13,16,17</sup>, could constitute a diffusion barrier at the ME/ARH border, using *Wisteria floribunda* agglutinin (WFA), the most widely used marker to visualize the PNN due to its affinity for chondroitin sulfate (CS) chains of PNN components<sup>28</sup>. Labeling for albumin and the PNN using WFA showed a link between the drop in albumin levels and the density of the PNN (Fig. 1d), which was confirmed by plotting albumin and PNN fluorescence intensities as a function of ventrodorsal distance (Supplementary Fig. 1c). To evaluate whether these CS glycans detected by WFA could play a role in the diffusion of circulating proteins, we analyzed albumin distribution in the ARH after stereotaxic injection of chondroitinase ABC (ChABC), which cleaves the CS chains of proteoglycans and can also digest hyaluronan, albeit less efficiently<sup>29</sup>. A ChABC dose-response experiment showed that, compared to 20mU, 5mU of ChABC infused into the ARH also led to the appearance of CS neopeptides which detection is linked to the enzymatic activity of ChABC<sup>30</sup> (Supplementary Fig. 2). Furthermore, at this low dose, ChABC did not alter the hyaluronan network (Supplementary Fig. 2), indicating that it does not have hyaluronidase activity thereby preserving the scaffolding on which the PNN components are attached. When 5mU of ChABC was infused into the ARH (ChABC<sup>5mU-ARH</sup>), PNN-positive surface was reduced by 25% after WFA labeling (Fig. 1e and Supplementary Fig. 2) and the diffusion of albumin into the ARH was greater than in control animals infused with PBS (PBS<sup>ARH</sup>) or heat-inactivated ChABC ( $\Delta$ ChABC<sup>ARH</sup>) (Fig. 1e, Supplementary Fig. 2) for which we did not detect the presence of CS neopeptides (Supplementary Fig. 2j). This suggests a specific role for CS chains carried by proteoglycans in the distribution of albumin in this brain region.

Searching for the identity of these proteoglycans in the ME/ARH by immunolabeling for PNN components, we observed that only aggrecan (ACAN) deposits were restricted to the ME/ARH border without spreading to the ME itself or more dorsally in the ARH in comparison with other PNN components more widely distributed in this brain region (Fig. 1f and Supplementary Fig. 3a–d). These ACAN deposits correspond to the diffusion barrier (Fig. 1g and Supplementary Fig. 1d) and the albumin concentration gradient observed across the ME and ARH (Fig. 1h), except in the aforementioned caudal extent of the subependymal ME/ARH border (Fig. 1c), where ACAN deposits avoid, but laterally cap, the fenestrated ME capillary loops reaching the ARH (Fig. 1i).

The match between the deposit of ACAN network and the abrupt decrease in albumin diffusion at the ME/ARH border prompted us to explore the role of ACAN in the diffusion of blood-borne molecules. We first used two independent mouse genetic models in which ACAN expression and deposition are altered: a hypomorphic mouse model for ACAN (*Acan*<sup>hyp</sup>), generated by the insertion of a *CreERT2* cassette into the 3'UTR of the *Acan* gene<sup>31</sup> and *Acan*<sup>IES/+</sup> heterozygote animals in which the *Acan* open reading frame was disrupted in exon 5<sup>32</sup>. In both models, *Acan* gene expression and deposition in the ME/ARH region were reduced (Fig. 2a, e) and coincided with a decrease in the CS glycan-positive surface labeled with WFA (Supplementary Fig. 4) without altering local blood-brain and blood-CSF barriers

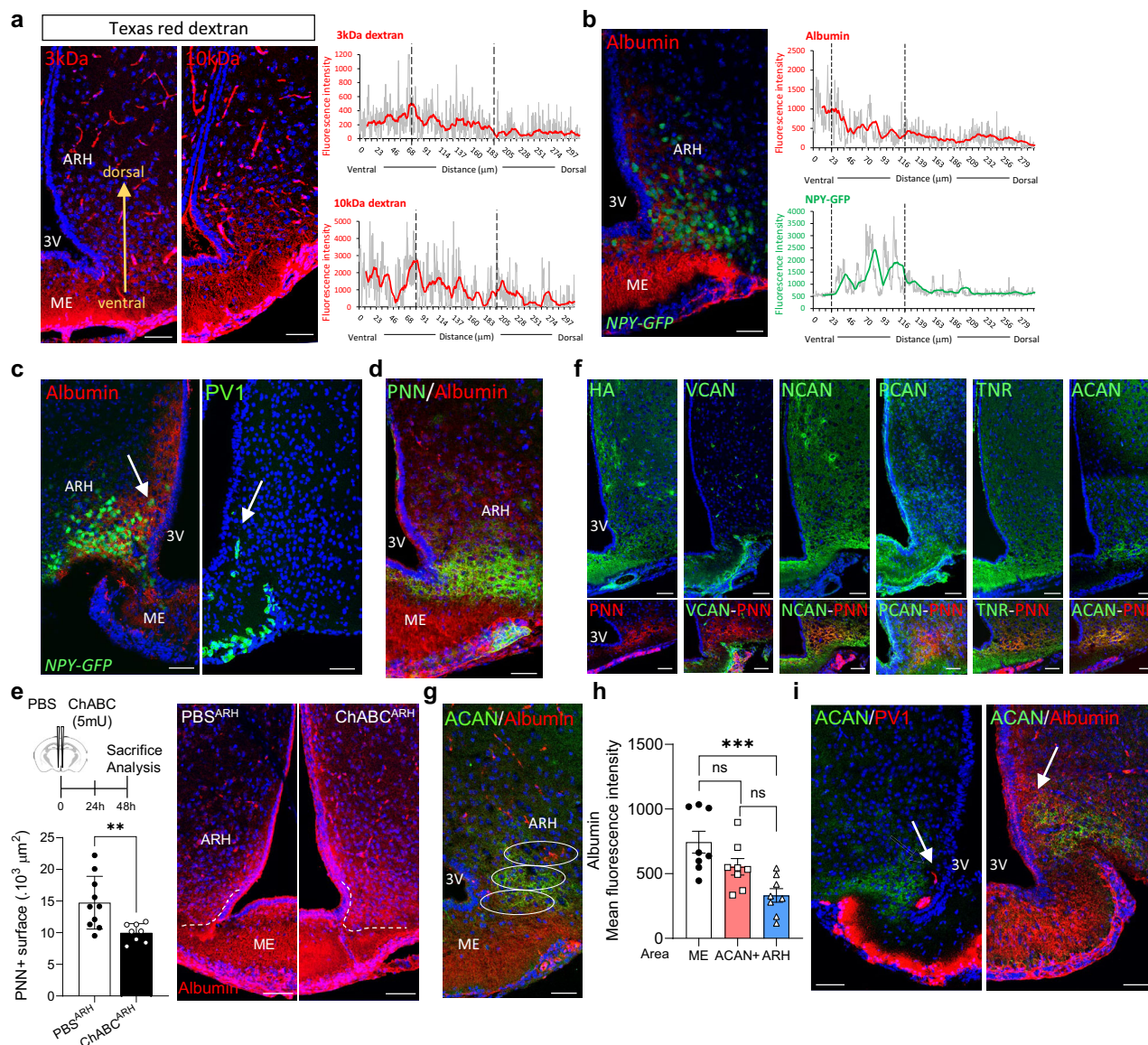


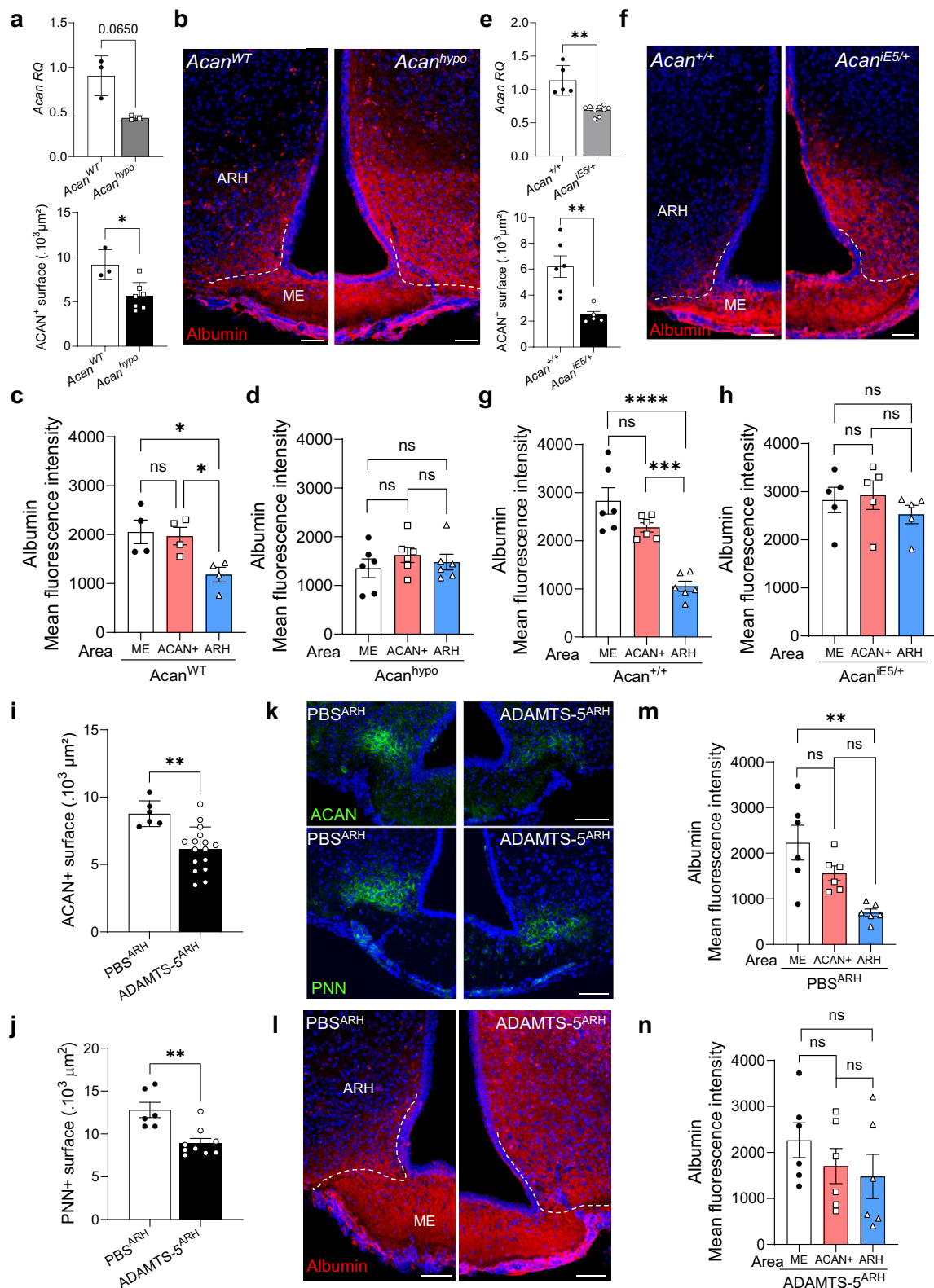
**Fig. 1 | The perineural net (PNN) at the ME/ARH boundary controls the passive diffusion of blood-borne molecules and consists of aggrecan (ACAN) deposits.**

**a** Left: Diffusion of intravenous Texas red dextran (left, 3 kDa; right, 10 kDa) in the median eminence (ME) and arcuate nucleus (ARH); Right: plot of dextran fluorescence intensity along the ME/ARH ventrodorsal axis. Experiments were performed two times with 5 mice per group. **b** Endogenous albumin immunolabeling (red) and NPY neurons (green) in *NPY-GFP* mice in the rostral (**b**) and caudal (**c**) ME. Plots in **b** show fluorescence intensity along the ventrodorsal axis. **c** Immunolabeling for albumin (red) and PV1 (a marker of endothelial fenestration, green) in the caudal ME. Left, the arrow indicates albumin diffusion along the 3V in the ARH; Right, the arrow points to a fenestrated vessel in the ARH. **d** Albumin (red) and PNN labeled using fluorescent *Wisteria floribunda* agglutinin (green) labeling. In **b**, **c** and **d**, experiments were performed two times. **e** Upper left, Illustration of the experimental procedure. Brain diagram was created with adobe illustrator 28.1. Quantification of PNN (bottom left, 5 mice, ARH analyzed bilaterally, mean and s.e.m. are

shown, two-tailed unpaired *t* test with Welch's correction (\*\*0.0059,  $t(11.58) = 3.365$ ) and extent of albumin (red) diffusion in ME/ARH of control-PBS and ChABC<sup>ARH</sup> mice (right). **f** Immunolabeling for hyaluronan (HA), versican (VCAN), neurocan (NCAN), phosphacan (PCAN), tenascin-R (TNR) and aggrecan (ACAN) in green and their overlay with the PNN (red, bottom panels). Experiments were performed two times. **g, h** Co-immunolabeling for albumin (red) and ACAN (green) and quantitative assessment of albumin fluorescence (**h**) in the ovals shown in **g** in 5 mice; 2 sections per mouse, means and s.e.m. are shown, one-way ANOVA test (\*\*0.0009,  $F(2, 21) = 9.212$ ). **i** Co-immunolabeling for albumin (red) and ACAN (green) or PV1 (red) in the caudal ME. Left, The arrow points to a fenestrated PV1-positive capillary entering the ARH; Right, the arrow indicates albumin diffusion in the ARH along the 3V. Experiments were repeated two times. Dashed lines in **e** delineate the ventral boundary of the ARH. ME: median eminence, ARH: hypothalamic arcuate nucleus, 3V: third ventricle. Scale bars: 50 μm. Source data are provided as a Source Data file.

(Supplementary Fig. 5). In *Acan*<sup>hypo</sup> and *Acan*<sup>IES/+</sup> mouse brain sections, albumin diffused into the ARH to a greater extent, leading to the disappearance of its gradient (Fig. 2b–d, f–h). However, since the marked reductions in weight and length<sup>31</sup> and perinatal lethality<sup>32</sup> observed in *Acan*<sup>hypo</sup> and *Acan*<sup>IES/IES</sup> mice, respectively, would render the analysis of metabolic parameters in these animals biased or impossible, we developed another model of ACAN destabilization at the ME/ARH border.

We stereotactically infused the aggrecanase ADAMTS-5 (A Disintegrin and Metalloproteinase with Thrombospondin motifs-5<sup>33</sup>) into the ARH of adult mice. ADAMTS-5 has been shown to possess the highest ACAN-degrading activity among the known aggrecanases, although it also cleaves versican and neurocan proteoglycans<sup>34</sup>. This approach was initially chosen over the use of *Acan* shRNA due to the very low turnover of aggrecan highlighted in cartilage (approximately 0.06 per year in normal human intervertebral discs, corresponding to



a half-life of 12 years<sup>35</sup>). This potential low turnover rate of aggrecan at the ME/ARH border could have rendered the knockdown of *Acan* ineffective in destabilizing the already-deposited ACAN protein in adult animals. When the ACAN network was acutely disrupted by stereotaxically injecting ADAMTS-5 into the ARH bilaterally (ADAMTS-5<sup>ARH</sup>), ACAN-positive surface was reduced by ~30% at the ME/ARH frontier after immunolabeling of ACAN protein core (Fig. 2i, k),

resulting expectedly in a decrease in the area covered by CS glycan labeled with WFA (Fig. 2j, k). This ACAN disruption led to an increase in albumin diffusion into the ARH and a flattening of its concentration gradient (Fig. 2l, m, n). These changes did not occur in control animals receiving a bilateral injection of PBS (PBS<sup>ARH</sup>) or infused with heat-inactivated ADAMTS-5 ( $\Delta$ ADAMTS-5<sup>ARH</sup>, Supplementary Fig. 6). Under our experimental conditions (100 ng of ADAMTS-5 per injection),

**Fig. 2 | Aggrecan deposits regulate blood-borne molecule distribution between the ME and the ARH.** **a–n** Quantification of *Acan* (**a, e**, upper panels, 3–7 mice, means and s.e.m. indicated, two-tailed unpaired *t* test with Welch's correction  $p = 0.065$ ,  $t(2.052) = 3.65$ ),  $^{**}p = 0.0095$ ,  $t(4.473) = 4.347$ ) and area of ACAN (**a, e** (lower panels, 3–4 mice, ARH analyzed bilaterally, mean and s.e.m. are shown, two-tailed unpaired *t* test  $^{*}p = 0.012$ ,  $t(8) = 3.25$ ; with Welch's correction  $^{**}p = 0.0049$ ,  $t(6.158) = 4.277$ ), **i** 3–8 mice, two-tailed unpaired *t* test,  $^{**}p = 0.0015$ ,  $t(20) = 3.67$ , **k**) and PNN (**j** 3–5 mice, two-tailed Mann–Whitney test,  $^{**}p = 0.0048$ , **l**) deposits, and quantification of albumin ventrodorsal distribution in the ME/ARH region (**b–d**, **f–h**, **l–n**) in *Acan*<sup>hyp0</sup> (**a–d**, 3 mice; left and right ARH/mice, mean and

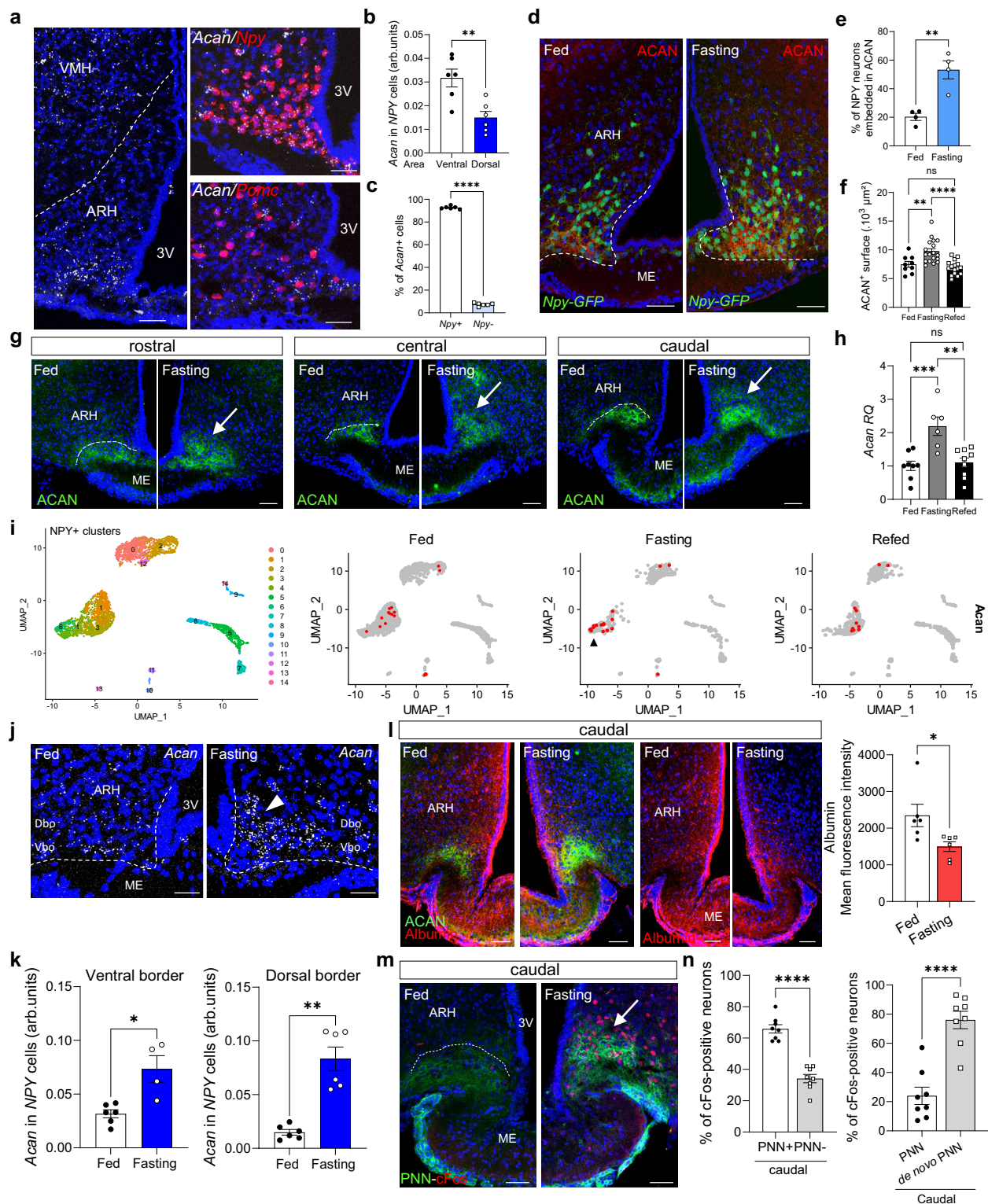
s.e.m. are shown, one-way ANOVA test, ME vs ARH  $^{*}p = 0.0271$ ; ACAN+ vs ARH  $^{*}p = 0.0443$ ,  $F(2, 9) = 6.161$ ), *Acan*<sup>if5/+</sup> (**e–h** 3 mice, left and right ARH/mice; means and s.e.m. are shown, one-way ANOVA test,  $^{****}p < 0.0001$ ;  $^{***}p = 0.0006$ ,  $F(2, 15) = 25.83$ ) and ADAMTS-5<sup>ARH</sup> (**i–n**; left and right ARH analyzed, means and s.e.m. are shown; **m, n** 5 mice, one-way ANOVA test,  $^{**}p = 0.0013$ , ACAN+ vs ARH  $p = 0.059$ ,  $F(2, 15) = 9.950$ ) mice and their control littermates. Dashed lines in **b, f** and **l** delineate the ventral boundary of the ARH. Scale bars: 50  $\mu\text{m}$ . ME median eminence, ARH hypothalamic arcuate nucleus. Source data are provided as a Source Data file.

immunolabeling for ADAMTS-5 confirms the presence of the enzyme in the ARH 48 h after its infusion (Supplementary Fig. 6). Furthermore, ADAMTS-5 treatment did not induce significant changes of HA, NCAN, PCAN or TNR deposition (Supplementary Fig. 7), likely due to a predominant aggrecanase activity at the administered dose. In addition, ADAMTS-5 infusion did not compromise the integrity of the blood-brain and blood-CSF barriers, as verified by tight-junction immunolabeling (ZO-1) either in ADAMTS-5<sup>ARH</sup> brain sections (Supplementary Fig. 8a) or after the infusion of ADAMTS-5 into the dorsomedial hypothalamus (ADAMTS-5<sup>DMH</sup>), which harbors dense ACAN deposits (Supplementary Fig. 8b). Indeed, in ADAMTS-5<sup>DMH</sup> mice, ACAN deposits were significantly reduced in the DMH without disrupting the blood-brain barrier as revealed by the retention of blood-borne 3 kDa fluorescent dextran in capillaries of the blood-brain barrier in the DMH (Supplementary Fig. 8b–e). The preservation of the blood-brain and blood-CSF barriers following ADAMTS-5 infusion indicate that the increased albumin diffusion into the ARH was mostly due to disrupted ACAN deposits at the ME/ARH.

Investigating the source of ACAN in fed mice, we observed using single and double in situ hybridization that the majority of *Acan*-expressing cells (~90%, Fig. 3c) were orexigenic NPY neurons lying at the ME/ARH interface in the ventral part of the ARH (Fig. 3a, b), and corresponding to the ~20% of NPY neurons embedded in ACAN, as seen in *Npy-GFP* transgenic mice (Fig. 3e). Because fasting is known to activate ARH neurons<sup>36</sup> and induces local morphological rearrangements<sup>37</sup>, we food-deprived *Npy-GFP* transgenic mice and discovered that ACAN deposition spread dorsally (Fig. 3d, f), embedding a greater proportion of NPY neurons than in fed mice (Fig. 3e). This dorsal extension of the ACAN network is observed throughout the anteroposterior axis of the ME/ARH (Fig. 3g and Supplementary Fig. 9a) and corresponds to the dorsal presence of CS glycan, as indicated by WFA labeling and the measurement of the PNN-positive surface all along the rostro-caudal axis of this brain region (Supplementary Fig. 9b–g). Accordingly, *Acan* transcript levels were upregulated in the ME/ARH in fasting animals (Fig. 3h). Subclustered cells from single cell RNA sequencing data of the ME/ARH region in fed and fasting conditions<sup>38</sup> with an *Npy* gene count greater than zero resulted in 15 clusters of NPY<sup>+</sup> cells, out of which clusters 1, 3, 4, and 6 were NPY neurons. In the fasting state, *Acan* expression selectively increases in cluster 6 which constitutes ~92% of cells expressing this transcript (Fig. 3i). This discrete subset of NPY neurons expressing *Acan* with fasting probably included the neuronal population in the dorsal ME/ARH border that also showed de novo expression of *Acan* in fasting mice, as revealed by in situ hybridization (Fig. 3j, k). Consistent with the dorsal extension of ACAN deposition observed in fasting mice along the rostro-caudal axis of the ME/ARH (Fig. 3g and Supplementary Fig. 9a), *Acan* transcript levels also showed an increase along the entire axis (Supplementary Fig. 10). To investigate the impact of this fasting-dependent dorsal extension of ACAN deposition on blood-borne molecule diffusion, we compared albumin distribution in the ME/ARH in fed and 16h-fasting mice. We observed that, compared to fed mice (Fig. 1c, i), albumin diffusion in the ARH was more restricted with fasting, especially in central and caudal regions of the ME/ARH where

albumin no longer leaked dorsally into the ARH along the wall of the third ventricle but rather remained concentrated at the level of the neurons newly embedded in ACAN in response to food deprivation (Fig. 3l and Supplementary Fig. 11). Since fasting is known to induce neuronal activation in the ARH<sup>39,40</sup>, we compared cFos protein expression as a marker of neuronal activation using immunolabeling<sup>41</sup> with the new deposition of the PNN after 16 h of food restriction. In fasting mice, at the caudal end of the ME/ARH, approximately 65% of cFos-positive neurons were surrounded by the PNN (Fig. 3m, n left panel), among them, 80% are located in the newly formed PNN (Fig. 3n right panel). This specific distribution of cFos-positive neurons was also observed in the central and rostral regions of the ME/ARH, although more moderately for this latter area where the number of fasting-induced activated neurons is lower (Supplementary Fig. 11c, d). This suggests that the newly deposited PNN, by restricting their diffusion, could potentially concentrate blood-borne metabolic signals in the vicinity of these neurons.

Because fasting induces the release into the circulation of the 3 kDa gut hormone ghrelin, which then activates NPY neurons of the ventromedial ARH to stimulate appetite<sup>39,40</sup>, we next investigated whether this ACAN-mediated diffusion barrier could influence the central response to ghrelin. To test this hypothesis, PBS<sup>ARH</sup> and ADAMTS-5<sup>ARH</sup> fed animals were intraperitoneally injected with ghrelin 30 min before examining neuronal activation using cFos immunolabeling. Intriguingly, while the overall number of ghrelin-induced cFos-positive neurons was reduced in the ventral ARH of ADAMTS-5<sup>ARH</sup> compared to PBS<sup>ARH</sup> animals, this number was significantly increased in the dorsal ARH (Fig. 4a, b). The equal number of cFos-positive neurons in the ARH of normally fed PBS<sup>ARH</sup> and ADAMTS-5<sup>ARH</sup> mice ruled out alterations of basal neuronal activation following ADAMTS-5 injection into the ARH (Fig. 4c, d), suggesting that the modifications observed are associated with a direct alteration of ghrelin signaling. Moreover, in the ventromedial nucleus of the hypothalamus (VMH), another brain region involved in the control of metabolism and adjacent to the ARH, the number of cFos-positive neurons remained unchanged between ADAMTS-5<sup>ARH</sup> and PBS<sup>ARH</sup> mice following ghrelin injection (Fig. 4a, e) despite a reduction in ACAN deposition in the VMH induced by aggrecanase infusion (Supplementary Fig. 12), indicating that major functional changes upon ACAN disruption were observed in the ARH. To verify that the changes in the pattern of neuronal activation in the ARH were the result of the increased diffusion and thus the dilution of the ghrelin signal due to the disruption of the ACAN network, we analyzed the diffusion of a marker of similar molecular weight, 3 kDa fluorescent dextran, into the ARH of ADAMTS-5<sup>ARH</sup> mice 5 min after dextran injection into the bloodstream. Compared to control PBS<sup>ARH</sup> mice, in which dextran spreads as a gradient into the ME/ARH (Fig. 4f, g), we observed that following ACAN disruption, 3kDa-dextran diffuses more uniformly throughout the ARH, resulting in the loss of its distribution gradient, similarly to the homogenous pattern of albumin in ADAMTS-5<sup>ARH</sup> mice (Fig. 2l, m, n). Taken together, these results indicate that the changed pattern of ghrelin-induced cFos expression in the ARH of ADAMTS-5<sup>ARH</sup> mice, compared to PBS<sup>ARH</sup> controls, is likely a result of the altered diffusion dynamics of molecules extravasating from ME fenestrated capillaries into the ARH parenchyma.



To evaluate whether this control of ghrelin diffusion by ARH ACAN deposits is physiologically relevant, we measured food intake in response to ghrelin injection in ADAMTS-5<sup>ARH</sup> fed animals. Ghrelin-induced food intake was significantly greater in ADAMTS-5 infused mice as compared to control PBS<sup>ARH</sup> animals (Fig. 4h). We also measured refeeding in 16h-fasting PBS<sup>ARH</sup> and ADAMTS-5<sup>ARH</sup> mice 2 days after aggreganase infusion and found that ADAMTS-5-injected mice ate more than controls (Fig. 4i), indicating that ACAN deposition plays a key role in the physiological adaptive response to fasting.

In summary, we show that the deposition of ACAN at the ME/ARH interface restrains the dorsolateral diffusion of blood-borne metabolic hormones such as ghrelin, and that its plastic remodeling plays a role in the adaptive response to fasting. Our study sheds light on the molecular composition and physiological role of this hitherto enigmatic diffusion barrier between the ME and the ARH, long known to restrict the free diffusion of blood-borne molecules extravasating from fenestrated ME microvessels<sup>5-12</sup>. Our previous studies have shown that tanyocytes, specialized hypothalamic glia of the ME/ARH that extend

**Fig. 3 | Remodeling of aggrecan (ACAN) deposits concentrates blood-borne molecules in the ventromedial ARH during fasting.** **a–c** In situ hybridization showing *Acan* expression (white) in *Npy* neurons (red) but not in POMC (red) neurons, *Acan* quantification in *Npy* positive cells (**b** 6 mice, means  $\pm$  s.e.m., two-tailed unpaired *t* test,  $^{**}p = 0.005$ ,  $t(10) = 3.638$ ) and percentage of cells co-expressing *Acan* and *Npy* (**c**, 6 mice, means  $\pm$  s.e.m., two-tailed unpaired *t* test,  $^{****}p < 0.0001$ ,  $t(10) = 108.2$ ). **d–k** ACAN (red, **d**, **f** (ACAN-positive surface measured in central sections of the ME/ARH), 8 mice, means  $\pm$  s.e.m., one way ANOVA test,  $^{**}p = 0.0049$ ,  $^{****}p < 0.0001$ ,  $F(2, 40) = 13.65$ ), green, **g** along the rostro-caudal axis), and *Acan* (**h**, **j**) expression in fasting and fed states. Six-nine mice, means and s.e.m. are shown, one-way ANOVA test,  $^{**}p = 0.0012$ ,  $^{***}p = 0.0007$ ,  $F(2, 20) = 11.92$ . Note that fasting increases the proportion of NPY neurons (green in **d** and **e**, 4 mice, means  $\pm$  s.e.m., two-tailed unpaired *t* test,  $p = 0.003$ ,  $t(6) = 4.850$ ) expressing *Acan* (**j**, **k**, 6 mice, means  $\pm$  s.e.m., ventral, two-tailed unpaired *t* test,  $^{**}p = 0.0049$ ,  $t(8) = 3.845$ ; dorsal, two-tailed Mann–Whitney test  $^{**}p = 0.0022$ , Dbo: Dorsal ME/ARH border; Vbo: ventral ME/ARH border, arrowhead in **j** shows neurons along the

wall of the third ventricle expressing *Acan* with fasting) and dorsal ARH ACAN deposition (red, **d**, green, **g**). Single-cell RNA sequencing data from GSE90806<sup>38</sup> are shown in **i**, **l**, **m**, endogenous albumin (red) and ACAN (green) co-immunolabeling (**l**) and PNN (green) and cFos (red) co-labeling (**m**) in fed and fasting mice in the caudal ME. **l** right, albumin fluorescent intensity measured in the ARH just above the ACAN deposit in fed and fasting mice (3 mice, left and right ARH analyzed, mean  $\pm$  s.e.m. indicated, two-tailed Mann–Whitney test,  $^{*}p = 0.015$ ). **n** percentage of cFos-positive neurons embedded in PNN (PNN+) or not (PNN-) in fasting mice in the caudal ME (left) or in de novo PNN (right) (4 mice, ARH bilaterally analyzed, mean  $\pm$  s.e.m. indicated, two-tailed unpaired *t* test,  $^{****}p < 0.0001$ , left,  $t(14) = 8.455$ ; right,  $t(14) = 6.144$ ). Dashed lines in **g** and **m** delineate the ventrodorsal boundary of the ARH; arrows in **g** and **m** show the dorsal extension of ACAN deposit. ME median eminence, ARH hypothalamic arcuate nucleus, VMH ventromedial nucleus of the hypothalamus, 3V: third ventricle. Scale bars: 50  $\mu$ m. Source data are provided as a Source Data file.

from the ependymal surface of the third ventricle to the plexus of fenestrated capillaries underlying the ME, form a barrier between the blood and CSF<sup>37</sup>. Although structural changes to this barrier modulate the access of blood-borne metabolic signals to ventromedial ARH neurons and, consequently, the adaptive response to acute nutritional challenges<sup>26,37</sup>, the process by which hunger signals such as circulating ghrelin selectively target more dorsal appetite-controlling NPY neurons bordering the wall of the third ventricle was unknown. The present work also demonstrates, intriguingly, that these NPY neurons, which are contacted by ME capillary loops<sup>3</sup> that become fenestrated in fasting animals by a VEGFA-dependent process set in motion by tanycytes<sup>37</sup>, or possibly by MCH neurons under other conditions<sup>42</sup>, themselves produce ACAN under food deprivation. The fenestrated ME capillary loops contacting these neurons could thus bypass the ACAN deposits at the ME/ARH border and provide a subpopulation of NPY neurons with direct access to blood-borne metabolic signals, whose diffusion would however be tightly controlled spatially and temporary by the de novo deposition of ACAN by these very neurons. It is interesting to note that the turnover of newly formed ACAN in the ventral ARH region at the ME/ARH border is rapid, resulting in an alternance between the presence and absence of ACAN in this very specific region as quickly as a change in nutritional status. In contrast, in cartilage, ACAN turnover is low, showing stability over several years<sup>35</sup>. This significant difference in stability between ACAN in cartilage and that in ventral ME/ARH border highlights the biological importance of ACAN at this border and potential functional differences.

The PNN-mediated concentration of blood-borne signals in the extracellular neighborhood of ARH neurons that can sense them may thus be an important aspect of the hypothalamic integration of and response to these signals. The fine-tuning of the density and plasticity of this unprecedented modulator of diffusion, and the physiological repercussions of the differential activation of distinct subpopulations of NPY or possibly other ARH neurons for the adaptive response to peripheral energy states are interesting questions that remain to be addressed.

## Methods

### Animals

7–12-week-old C57BL/6J male mice from Charles River were group-housed in a controlled environment (12 h:12 h light-dark cycle, humidity 40–60% and temperature  $21 \pm 2$  °C) and had *ad libitum* access to water and standard rodent chow diet unless specified in the experimental procedure. During accommodation, animals were fed with Safe<sup>®</sup>03 (Safe Diets). Brain tissues from the hypomorphic *Acan*<sup>tm1(cre/ERT2)Cm</sup> (JAX stock #019148<sup>31,43</sup>) mice (hereinafter *Acan*<sup>hypo</sup>) or *Acan*<sup>CreERT2/CreERT2</sup>, 3 to 6 months of age) and from the *Acan*<sup>fls/+</sup> heterozygous knockout mice (3 to 6 months of age) were provided by the

Musculoskeletal University Center of Munich (MUM), Germany. Functional knockout of the *Acan* allele was generated by disrupting the open reading frame in exon 5 in embryonic stem cells (Toshi Oohashi, Okayama University, Japan and Attila Aszodi, MUM, Germany). *Npy-GFP* transgenic mice (3 to 6 months) were from the Jackson Laboratory (JAX stock # 006417). Experiments were conducted following protocols approved by the French Ethics Committee (CEEA75, APAFIS number: APAFIS#29172).

### Intravenous injection of fluorescent dextran

3 kDa and 10 kDa Texas red lysine-fixable dextrans (ThermoFisher Scientific, D3328, D1863, respectively) were injected at 6  $\mu$ M and 3  $\mu$ M, respectively in the retro-orbital sinus of mice (100  $\mu$ l/injection) previously anesthetized with isoflurane. Five minutes after injection, mice were sacrificed by decapitation and brains immediately fixed in 4% paraformaldehyde (PFA) for further analyses.

### Fasting and refeeding experiments

C57BL6/J male mice were individually housed and nourished overnight or fasted just before the dark phase for 16 h. For refeeding mice, after an overnight fasting period, they were given a standard diet for 2 or 4 h before sacrifice.

### Stereotaxic injection into the mediobasal hypothalamus

During surgery, mice were maintained over a heating pad and eyes were protected with ocular gel (Ocrygel). Mice were stereotaxically microinjected with ChABC (5mU or 20mU/100 nl, 100 nl/injection, Sigma, C3667), or ADAMTS-5 (1  $\mu$ g/ $\mu$ L, 100 nl/injection, R&D system) under anaesthesia with isoflurane with a stereotaxic apparatus (KopF Instrument, model 963/962) using the stereotaxic coordinates:  $-1.1$  mm posterior to Bregma,  $\pm 0.3$  mm lateral and  $-6$  mm below the skull surface for ARH injection. Stereotaxic coordinates:  $-1.1$  mm posterior to Bregma,  $\pm 0.3$  mm lateral and  $-5$  mm below the skull surface were used for DMH infusion. Injections were given bilaterally at a rate of 25 nl/min with a KD Scientific Legato130 using a 2  $\mu$ l Neuros Hamilton syringe equipped with 30 Gauge blunt needle. Control animals were injected bilaterally with PBS or heat-inactivated ChABC ( $\Delta$ ChABC, 5mU/100 nl, 100 nl/injection, previously heated to 85 °C during 45 min<sup>14</sup>) or heat-inactivated ADAMTS-5 ( $\Delta$ ADAMTS-5, 1 mg/ml, 100 nl/injection, heated to 85 °C during 45 min<sup>14</sup>) using the same stereotaxic coordinates. After surgery, mice were housed individually for 48 h before ghrelin challenge and food intake measurement.

### Ghrelin challenge in ADAMTS-5 centrally injected mice

Forty-eight hours after stereotaxic injection, mice were intraperitoneally injected with rat ghrelin (2 mg/kg in 0.9% NaCl, R&D,



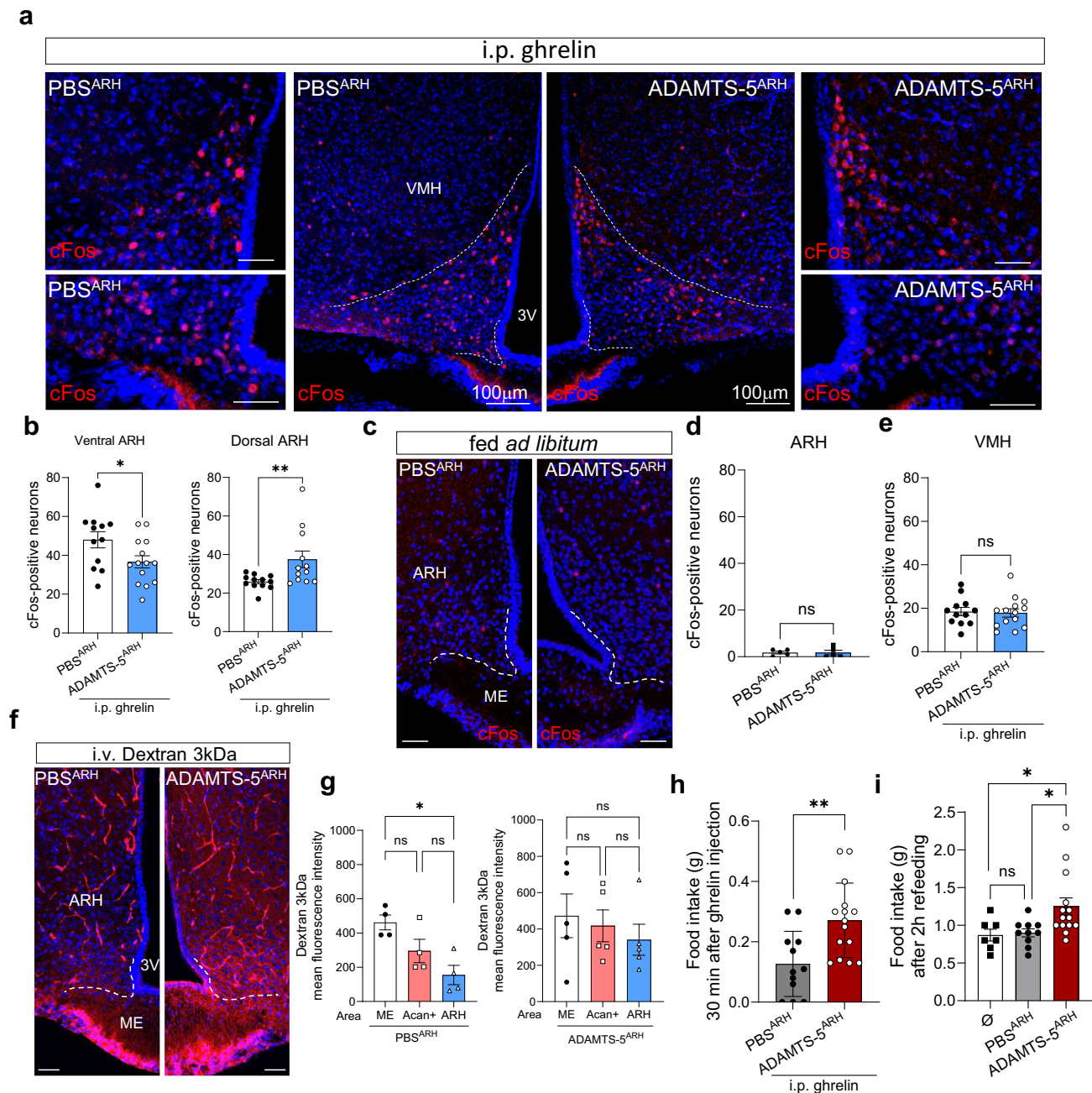


**Fig. 4 | Aggrecan deposition is involved in the adaptive response to fasting.**

**a, b** Ghrelin-induced cFos expression in the ventral and dorsal ARH of PBS<sup>ARH</sup> and ADAMTS-5<sup>ARH</sup> wildtype mice (**b**, PBS<sup>ARH</sup>  $n = 6$ , ADAMTS-5<sup>ARH</sup>  $n = 7$ , ARH analyzed bilaterally, ventral: two-tailed unpaired  $t$  test,  $*p = 0.0367$ ,  $t(24) = 2.212$ ; dorsal: two-tailed Mann–Whitney test,  $**p = 0.0085$ ). **c, d** Immunolabeling for cFos (red) and counts of cFos-positive neurons in the ARH of PBS<sup>ARH</sup> and ADAMTS-5<sup>ARH</sup> mice fed *ad libitum*. 3–5 mice, ARH analyzed bilaterally, means and s.e.m. indicated, two-tailed unpaired  $t$  test. **e** Number of cFos-positive neurons in the VMH of PBS<sup>ARH</sup> and ADAMTS-5<sup>ARH</sup> mice treated with ghrelin. 7 mice, ARH analyzed bilaterally, means and s.e.m. indicated, two-tailed unpaired  $t$  test. **f, g** Intravenous 3 kDa Texas red dextran diffusion in PBS<sup>ARH</sup> and ADAMTS-5<sup>ARH</sup> mice (3 mice, means and s.e.m. are

shown, ARH analyzed bilaterally, one-way ANOVA test,  $*p = 0.01$ ,  $F(2, 9) = 7.303$ ). **h, i** Food intake (**h**) and refeeding (**i**) (**h**, in 30-min ghrelin-injected; 12–14 mice, means and s.e.m. are shown, two-tailed unpaired  $t$  test,  $**p = 0.004$ ,  $t(25) = 3.192$ ) and 16-h fasting (**i**, 7–14 mice, ∅ represents uninjected mice; means and s.e.m. are shown, Kruskal–Wallis test, ∅ versus ADAMTS-5<sup>ARH</sup>  $*p = 0.039$ ; PBS<sup>ARH</sup> versus ADAMTS-5<sup>ARH</sup>  $*p = 0.033$ ) PBS<sup>ARH</sup>, ADAMTS-5<sup>ARH</sup> and wildtype mice. Dashed lines indicated the boundaries of the ARH considered for quantification. ME median eminence, ARH hypothalamic arcuate nucleus, VMH ventromedial nucleus of the hypothalamus. 3V: third ventricle. Scale bars: 50 μm except where indicated. Source data are provided as a Source Data file.

#1465) at 11am. Thirty minutes later, food intake was measured before sacrifice by decapitation after anaesthesia with isoflurane. Brains were collected and fixed overnight at 4 °C in 4% PFA then cryoprotected (see below) before processing for cryosectioning and immunolabeling.

#### Brain processing and cryosectioning for immunolabeling or RNA in situ hybridization

For immunolabeling, brains were fixed in 4% PFA overnight at 4 °C before cryoprotection in 15% and 30% sucrose in PBS overnight at 4 °C. Cryoprotected brains were frozen in OCT on dry ice and stored at

–80 °C until cryosectioning. For RNA in situ hybridization, fresh brains were immediately frozen in OCT after harvesting and stored at –80 °C before cryosectioning. For cryosection, frozen brains were placed at –20 °C overnight for equilibration and cut on a Leica CM3050S cryostat at 14 µm (sections on slides for fresh frozen brains) or at 35 µm (floating sections for fixed frozen brains). Slides were kept at –20 °C and floating sections were stored in 0.05% Na<sub>2</sub>N<sub>3</sub> in PBS at 4 °C until processing.

### Immunolabeling

Floating sections or sections on slides were treated with blocking buffer containing 5% normal donkey serum and 0.3% Triton X-100 (when necessary) in PBS for 1 h at room temperature before incubation with WFA (Wisteria Floribunda Agglutinin, 1/500, Sigma, L1516-2MG), HABP (hyaluronic binding protein, 1/50, Millipore, 385911) or primary antibodies (anti-vimentin, 1/2000, BioLegend, 919101; anti-POMC, 1/1000, Phoenix pharmaceutical, H-029-30; anti-aggrecan, 1/500, Millipore, AB1031; anti-neurocan, 1/500, R&D system, AF5800; anti-versican antibody anti-VC<sup>44</sup>, 1/250; anti-tenascin-R, 1/50, R&D System, AF3865; anti-phosphacan, 5 mg/ml, DSHB, 3F8-S, anti-albumin, 1/500, abcam, ab8940; anti-cFOS, 1/1000, Synaptic Systems, 226003, anti-chondroitin 4 sulfate (CS neoepitope), 1/1000, Sigma Aldrich, MAB2030) in 0.3% Triton X-100/PBS for 48 h at 4 °C. For phosphacan labeling, Fab fragment of donkey anti-mouse IgG (Jackson Laboratories, 715-007-003) diluted 1/500 was added to the blocking buffer. For CS neoepitope immunolabeling, sections were blocked with M.O.M blocking reagent (VectorLabs) and incubated with M.O.M protein concentrate following the manufacturer instructions. Sections were then rinsed 3 times 10 min in PBS before incubation for 2 h at room temperature with streptavidin Alexa 488/568 (1/1000, Invitrogen), or anti-chicken alexa 488 (1/500, Invitrogen) or anti-rabbit Alexa 488/568/647 (1/500, Invitrogen) or anti-sheep Alexa 488/568/647 (1/500, Invitrogen) or anti-goat Alexa 488 (1/500, Invitrogen) or Alexa 568 anti-mouse IgG (1/500, Invitrogen) diluted in 0.3% Triton X-100/PBS or in PBS containing M.O.M protein concentrate. For cFOS immunolabeling, after incubation with primary antibody, sections were incubated with donkey anti-rabbit biotinylated antibody (1/500, Jackson Immuno Research) diluted in PBS containing 0.3% Triton X-100 and 0.25% bovine serum albumin for 90 min at room temperature. Sections were then washed and treated for 2 h at room temperature with streptavidin conjugated to Alexa 568 (1/500, Invitrogen) diluted in 0.3% Triton X-100, 0.25% bovine serum albumin, PBS. For ZO-1 and type IV collagen co-immunolabeling or PV-1 and ACAN co-immunolabeling, thin sections (14 µm) on slides were fixed with 50% acetone/50% methanol for 1 min at –20 °C and then dried for 10 min at room temperature. For ADAMTS-5 immunolabeling, thin sections (14 µm) on slides were fixed 10 min in 4% PFA. After three washes of 10 min with PBS, sections were treated with blocking buffer containing 5% of donkey serum and 0.3% Triton in PBS for 1 h at room temperature before incubation with primary antibodies (anti-ZO-1, 1/500, Invitrogen, 61-7300; anti-Coll-IV, 1/500, Millipore, AB769, anti-PV-1, 1/250, BD Biosciences clone MECA-32; anti-aggrecan, 1/500, Millipore, AB1031 or anti-ADAMTS-5, 1/100, abcam, ab41037) overnight at 4 °C. Sections were then rinsed three times 10 min in PBS and incubated with donkey anti-goat Alexa 594 (1/500, Invitrogen) and donkey anti-rabbit Alexa 488 (1/500, Invitrogen) or donkey anti-rat Alexa 594 (1/500, Invitrogen) and donkey anti-rabbit Alexa 488 (1/500, Invitrogen) or with biotinylated donkey anti-rabbit diluted in 4% goat serum and 0.3% Triton in PBS for 2 h at room temperature. For ADAMTS-5 staining, sections were then treated with streptavidin as described above. For all labelings, after washes, sections were rinsed with PBS, counterstained 5 min in DAPI (1/5000 in PBS, 5 mg/mL), washed in PBS and mounted in Mowiol.

### RNA in situ hybridization

Multiplex RNA in situ hybridizations were performed on fresh frozen brain sections using RNAscope technology and following the manufacturer instructions (RNAscope Multiplex Fluorescent Reagent Kit V2 Assay). Probes for *Acan* (Mm-Acan C1, ref: 439101), *Npy* (Mm-NPY C2, ref: 313321-C2) and *Pomc* (Mm-POMC C2, ref: 314081-C2) were provided by ACD Biotechne as well as positive control (targeting housekeeping genes) or negative control (targeting bacterial genes) probes.

### RNA extraction, reverse transcription and qPCR

Mice were sacrificed and brains were harvested in RNAlater (10 ml/brain, Qiagen) for microdissection. A brain region corresponding to the median eminence and the arcuate nucleus was microdissected under a stereomicroscope (Leica M55) and immediately frozen in liquid nitrogen until processing.

RNAs were extracted from microdissected brain areas using the RNeasy® Mini Kit from Qiagen (ref: 74104) or E.Z.N.A. Total RNA Kit II (Omega Bio-Tek, R6934-02) and following the manufacturer's instructions. Total RNA (0.5 µg or 1 µg) were reverse transcribed using the HighCapacity cDNA Reverse Transcription Kit (Applied Biosystems) and following the manufacturer's instructions. Relative quantification was performed using Taqman Gene Expression Master Mix and specific Taqman probes (*aggrecan*, Mm00545794\_m1; *actin*, Mm00607939\_s1) using a StepOne real-time PCR system. Expression levels of mRNA were quantified using the 2<sup>-ΔΔCT</sup> method and normalized to β-actin.

### Quantification of aggrecan fluorescence intensity, aggrecan transcript, NPY neurons embedded in ACAN and cFOS+ neurons

Quantifications were performed on images taken by a LSM 710 or a LSM 980 confocal microscope and after in situ hybridization or immunolabeling of brain sections in different experimental conditions. Rostral, central and caudal brain sections were classified as indicated in Supplementary Fig. 13 and using the scalable brain atlas<sup>45</sup>. Albumin, aggrecan, NPY, PNN fluorescence intensities were determined using Zeiss Zen software. Fluorescence background was subtracted from raw data. For RNAscope® quantifications, single plane acquisitions from confocal microscopy were imported into Fiji and processed as follows: the regions of interest were manually delimited with the freehand tool. The NPY signal was thresholded, and the resulting segmentation was used as a mask to extract the ACAN RNAscope® signal in NPY+ cells only. Finally, the ACAN RNAscope® signal in NPY+ cells was thresholded and measured as a density of pixels, before normalization to the DAPI nuclear staining. The quantification process was automated using a Fiji macro, and thresholds for each channel were kept identical for all images.

cFOS+ neurons and ACAN-embedded NPY neurons were quantified by counting on images of immunolabeling and delineating the dorsal or ventral ARH regions as shown in Supplementary Fig. 13. The total numbers of NPY-positive neurons were counted as well as the NPY-positive neurons enwrapped in ACAN deposition to calculate the percentage of ACAN-embedded neurons.

### Re-analysis of single cell RNA sequencing data

The pre-processed gene counts and the corresponding meta-data from single-cell RNA sequencing of ME/ARH region of the hypothalamus were retrieved from Gene expression omnibus (GEO) with the accession number GSE90806<sup>38</sup>. The data was read and reanalysed using Seurat version 4.1.1, a toolkit for single cell genomics using R version 4.2.1. The Npy<sup>+</sup> cells (Npy>0) were then subclustered and grouped based on three diet conditions of 'fed', 'fasting' and 'refed'. The percentage of cells constituting Npy<sup>+</sup> cell clusters and the expression of *Acan* in Npy<sup>+</sup> cells was determined for fed, fasting and refed conditions. The standard Seurat functions were used for the visualization of

clusters. UMAP\_1 and UMAP\_2 represent the two-dimensional coordinate space of cells clustered by similarity in their gene expression.

### Statistical analysis

The data are presented as means and standard errors of the mean. All statistical analyses were performed using the software GraphPad Prism version 10.2.2 (GraphPad, San Diego, CA). The normal distribution of the samples was tested using the Shapiro-Wilk test. To compare two groups with normal distributions and no significant difference in variances, an unpaired Student *t* test was used. If the distribution of the samples was normal but there was a significant difference in variances, the Welch test was chosen. In the case of a non-Gaussian distribution of samples, the Mann-Whitney test was performed. Comparison of three or more groups with a normal distribution was performed with a one-factor analysis of variance (ANOVA) test with Tukey's multiple comparisons. If the distribution of samples was not Gaussian or the number of samples was too small to assume normality, the Kruskal-Wallis test followed by Dunn's multiple comparison was preferred. Values were excluded from statistical analyses when ACAN or PNN disruption was not confirmed by labeling on brain sections.  $P < 0.05$  were considered statistically significant. \* $p < 0.05$ ; \*\* $p < 0.01$ ; \*\*\* $p < 0.001$ ; \*\*\*\* $p < 0.0001$ .

### Reporting summary

Further information on research design is available in the Nature Portfolio Reporting Summary linked to this article.

### Data availability

All materials used are available from the authors or from standard commercial sources specified in the manuscript. We used publicly accessible dataset of single-cell RNA sequencing of ME/ARH region of the hypothalamus from Gene expression omnibus (GEO) with the accession number [GSE90806](https://www.ncbi.nlm.nih.gov/geo/query/acc.cgi?acc=GSE90806). Source data are provided with this paper.

### References

- Jais, A. & Brüning, J. C. Arcuate nucleus-dependent regulation of metabolism-pathways to obesity and diabetes mellitus. *Endocr. Rev.* **43**, 314–328 (2022).
- Timper, K. & Brüning, J. C. Hypothalamic circuits regulating appetite and energy homeostasis: pathways to obesity. *Dis. Model Mech.* **10**, 679–689 (2017).
- Ciofi, P. et al. Brain-endocrine interactions: a microvascular route in the mediobasal hypothalamus. *Endocrinology* **150**, 5509–5519 (2009).
- Olofsson, L. E., Unger, E. K., Cheung, C. C. & Xu, A. W. Modulation of AgRP-neuronal function by SOCS3 as an initiating event in diet-induced hypothalamic leptin resistance. *Proc. Natl. Acad. Sci. USA* **110**, E697–E706 (2013).
- Morita, S. & Miyata, S. Accessibility of low-molecular-mass molecules to the median eminence and arcuate hypothalamic nucleus of adult mouse. *Cell Biochem. Funct.* **31**, 668–677 (2013).
- Broadwell, R. D., Balin, B. J., Salzman, M. & Kaplan, R. S. Brain-blood barrier? Yes and no. *Proc. Natl. Acad. Sci. USA* **80**, 7352–7356 (1983).
- Shaver, S. W., Pang, J. J., Wainman, D. S., Wall, K. M. & Gross, P. M. Morphology and function of capillary networks in subregions of the rat tuber cinereum. *Cell Tissue Res.* **267**, 437–448 (1992).
- Ciofi, P. The arcuate nucleus as a circumventricular organ in the mouse. *Neurosci. Lett.* **487**, 187–190 (2011).
- Rodríguez, E. M., Blázquez, J. L. & Guerra, M. The design of barriers in the hypothalamus allows the median eminence and the arcuate nucleus to enjoy private milieus: the former opens to the portal blood and the latter to the cerebrospinal fluid. *Peptides* **31**, 757–776 (2010).
- Mullier, A., Bouret, S. G., Prevot, V. & Dehouck, B. Differential distribution of tight junction proteins suggests a role for tanycytes in blood-hypothalamus barrier regulation in the adult mouse brain. *J. Comp. Neurol.* **518**, 943–962 (2010).
- Martinez, J. L. & Koda, L. Penetration of fluorescein into the brain: a sex difference. *Brain Res.* **450**, 81–85 (1988).
- Wsniewski, H. & Olszewski, J. Vascular permeability in the area postrema and hypothalamus. a study using iodinated radioactive albumin. *Neurology* **13**, 885–894 (1963).
- Mirzadeh, Z. et al. Perineuronal net formation during the critical period for neuronal maturation in the hypothalamic arcuate nucleus. *Nat. Metab.* **1**, 212–221 (2019).
- Alonge, K. M. et al. Hypothalamic perineuronal net assembly is required for sustained diabetes remission induced by fibroblast growth factor 1 in rats. *Nat. Metab.* **2**, 1025–1033 (2020).
- Horii-Hayashi, N., Sasagawa, T., Matsunaga, W. & Nishi, M. Development and structural variety of the chondroitin sulfate proteoglycans-contained extracellular matrix in the mouse brain. *Neural Plast.* **2015**, 256389 (2015).
- Horii-Hayashi, N., Sasagawa, T. & Nishi, M. Insights from extracellular matrix studies in the hypothalamus: structural variations of perineuronal nets and discovering a new perifornical area of the anterior hypothalamus. *Anat. Sci. Int.* **92**, 18–24 (2017).
- Pócsai, K. & Kálmán, M. Extracellular matrix components mark the territories of circumventricular organs. *Neurosci. Lett.* **566**, 36–41 (2014).
- Testa, D., Prochiantz, A. & Di Nardo, A. A. Perineuronal nets in brain physiology and disease. *Semin. Cell Dev. Biol.* **89**, 125–135 (2019).
- Härtig, W. et al. Cortical neurons immunoreactive for the potassium channel Kv3.1b subunit are predominantly surrounded by perineuronal nets presumed as a buffering system for cations. *Brain Res.* **842**, 15–29 (1999).
- Beurdeley, M. et al. Otx2 binding to perineuronal nets persistently regulates plasticity in the mature visual cortex. *J. Neurosci.* **32**, 9429–9437 (2012).
- Bouret, S. G., Draper, S. J. & Simerly, R. B. Trophic action of leptin on hypothalamic neurons that regulate feeding. *Science* **304**, 108–110 (2004).
- Zhang, N. et al. Hypothalamic perineuronal nets are regulated by sex and dietary interventions. *Front Physiol.* **12**, 714104 (2021).
- Lufano, D. et al. Ghrelin binding to serum albumin and its biological impact. *Mol. Cell Endocrinol.* **436**, 130–140 (2016).
- Patterson, M., Murphy, K. G., le Roux, C. W., Ghatei, M. A. & Bloom, S. R. Characterization of ghrelin-like immunoreactivity in human plasma. *J. Clin. Endocrinol. Metab.* **90**, 2205–2211 (2005).
- Venema, W. et al. Ciliary neurotrophic factor acts on distinctive hypothalamic arcuate neurons and promotes leptin entry into and action on the mouse hypothalamus. *Front Cell Neurosci.* **14**, 140 (2020).
- Schaeffer, M. et al. Rapid sensing of circulating ghrelin by hypothalamic appetite-modifying neurons. *Proc. Natl. Acad. Sci. USA* **110**, 1512–1517 (2013).
- Nicholson, C. & Hrabětová, S. Brain extracellular space: the final frontier of neuroscience. *Biophys. J.* **113**, 2133–2142 (2017).
- Härtig, W., Brauer, K. & Brückner, G. Wisteria floribunda agglutinin-labelled nets surround parvalbumin-containing neurons. *Neuroreport* **3**, 869–872 (1992).
- Lin, R., Kwok, J. C. F., Crespo, D. & Fawcett, J. W. Chondroitinase ABC has a long-lasting effect on chondroitin sulphate glycosaminoglycan content in the injured rat brain. *J. Neurochem.* **104**, 400–408 (2008).
- Brückner, G. et al. Acute and long-lasting changes in extracellular-matrix chondroitin-sulphate proteoglycans induced by injection of chondroitinase ABC in the adult rat brain. *Exp. Brain Res.* **121**, 300–310 (1998).
- Alberston, P. et al. Aggrecan hypomorphism compromises articular cartilage biomechanical properties and is associated with

- increased incidence of spontaneous osteoarthritis. *Int. J. Mol. Sci.* **20**, E1008 (2019).
32. Empere, M. et al. Aggrecan governs intervertebral discs development by providing critical mechanical cues of the extracellular matrix. *Front Bioeng. Biotechnol.* **11**, 1128587 (2023).
  33. Verma, P. & Dalal, K. ADAMTS-4 and ADAMTS-5: key enzymes in osteoarthritis. *J. Cell Biochem* **112**, 3507–3514 (2011).
  34. Kintakas, C. & McCulloch, D. R. Emerging roles for ADAMTS5 during development and disease. *Matrix Biol.* **30**, 311–317 (2011).
  35. Sivan, S. S. et al. Aggrecan turnover in human intervertebral disc as determined by the racemization of aspartic acid. *J. Biol. Chem.* **281**, 13009–13014 (2006).
  36. Riediger, T., Bothe, C., Becskei, C. & Lutz, T. A. Peptide YY directly inhibits ghrelin-activated neurons of the arcuate nucleus and reverses fasting-induced c-Fos expression. *Neuroendocrinology* **79**, 317–326 (2004).
  37. Langlet, F. et al. Tanycytic VEGF-A boosts blood-hypothalamus barrier plasticity and access of metabolic signals to the arcuate nucleus in response to fasting. *Cell Metab.* **17**, 607–617 (2013).
  38. Campbell, J. N. et al. A molecular census of arcuate hypothalamus and median eminence cell types. *Nat. Neurosci.* **20**, 484–496 (2017).
  39. Wang, L., Saint-Pierre, D. H. & Taché, Y. Peripheral ghrelin selectively increases Fos expression in neuropeptide Y - synthesizing neurons in mouse hypothalamic arcuate nucleus. *Neurosci. Lett.* **325**, 47–51 (2002).
  40. Hewson, A. K. & Dickson, S. L. Systemic administration of ghrelin induces Fos and Egr-1 proteins in the hypothalamic arcuate nucleus of fasted and fed rats. *J. Neuroendocrinol.* **12**, 1047–1049 (2000).
  41. Sagar, S. M., Sharp, F. R. & Curran, T. Expression of c-fos protein in brain: metabolic mapping at the cellular level. *Science* **240**, 1328–1331 (1988).
  42. Jiang, H. et al. MCH neurons regulate permeability of the median eminence barrier. *Neuron* **107**, 306–319.e9 (2020).
  43. Henry, S. P. et al. Generation of aggrecan-CreERT2 knockin mice for inducible Cre activity in adult cartilage. *Genesis* **47**, 805–814 (2009).
  44. Foulcer, S. J. et al. Determinants of versican-V1 proteoglycan processing by the metalloproteinase ADAMTS5. *J. Biol. Chem.* **289**, 27859–27873 (2014).
  45. Bakker, R., Tiesinga, P. & Kötter, R. The scalable brain atlas: instant web-based access to public brain atlases and related content. *Neuroinformatics* **13**, 353–366 (2015).
- ANR-20-CE14-0046 to C.Q. Doctoral fellowships from the University of Lille to L.K.-N. and S.K.

### Author contributions

L.K.-N., S.K. and V.M. conceived the project. L.K.-N., S.K., P.A., I.M.-C., S.N., F.S., T.L., C.Q., J.D. and V.M. planned and performed experiments. L.K.-N., S.K., P.A., I. M.-C, S.N., F.S., S.B., P.C., J.D., V.P. and V.M. analyzed the results. P.A., S.A., A.A. provided materials. S.A., S.B., A.A., S.R., P.C., J.D., V.P. and V.M. wrote the manuscript.

### Competing interests

The authors declare no competing interests.

### Additional information

**Supplementary information** The online version contains supplementary material available at <https://doi.org/10.1038/s41467-024-50798-9>.

**Correspondence** and requests for materials should be addressed to Virginie Mattot.

**Peer review information** *Nature Communications* thanks the anonymous reviewers for their contribution to the peer review of this work. A peer review file is available.

**Reprints and permissions information** is available at <http://www.nature.com/reprints>

**Publisher's note** Springer Nature remains neutral with regard to jurisdictional claims in published maps and institutional affiliations.

**Open Access** This article is licensed under a Creative Commons Attribution-NonCommercial-NoDerivatives 4.0 International License, which permits any non-commercial use, sharing, distribution and reproduction in any medium or format, as long as you give appropriate credit to the original author(s) and the source, provide a link to the Creative Commons licence, and indicate if you modified the licensed material. You do not have permission under this licence to share adapted material derived from this article or parts of it. The images or other third party material in this article are included in the article's Creative Commons licence, unless indicated otherwise in a credit line to the material. If material is not included in the article's Creative Commons licence and your intended use is not permitted by statutory regulation or exceeds the permitted use, you will need to obtain permission directly from the copyright holder. To view a copy of this licence, visit <http://creativecommons.org/licenses/by-nc-nd/4.0/>.

© The Author(s) 2024

### Acknowledgements

The authors would like to thank the PLBS UAR 2014 – US41, Dr Gaëtan Ternier, Margot Ban and Clara Soncin for technical assistance. ERC Synergy WATCH, No 810331 to V.P., ANR-21-CE14-0041 to V.M. and J.D.,